

## Fracton critical point at a higher-order topological phase transition


Yizhi You,<sup>1</sup> Julian Bibo,<sup>2,3</sup> Frank Pollmann,<sup>2,3</sup> and Taylor L. Hughes<sup>4</sup>

<sup>1</sup>*Princeton Center for Theoretical Science, Princeton University, Princeton, New Jersey 08544, USA*

<sup>2</sup>*Department of Physics, Technical University of Munich, 85748 Garching, Germany*

<sup>3</sup>*Munich Center for Quantum Science and Technology (MQCST), D-80799 Munich, Germany*

<sup>4</sup>*Department of Physics and Institute for Condensed Matter Theory, University of Illinois at Urbana-Champaign, Champaign, Illinois 61801, USA*

 (Received 19 February 2021; revised 5 October 2022; accepted 17 October 2022; published 15 December 2022)

The theory of quantum phase transitions separating different phases with distinct symmetry patterns at zero temperature is one of the foundations of modern quantum many-body physics. Here we demonstrate that the existence of a two-dimensional topological phase transition between a higher-order topological insulator (HOTI) and a trivial Mott insulator with the same symmetry eludes this paradigm. We present a theory of this quantum critical point (QCP) driven by the fluctuations and percolation of the domain walls between a HOTI and a trivial Mott insulator region. Due to the spinon zero modes that decorate the rough corners of the domain walls, the fluctuations of the phase boundaries trigger a spinon-dipole hopping term with fracton dynamics. Hence we find that the QCP is characterized by a critical dipole liquid theory with subsystem U(1) symmetry and the breakdown of the area law entanglement entropy which exhibits a logarithmic enhancement:  $L \ln(L)$ . Using the density matrix renormalization group method, we analyze the dipole stiffness together with the structure factor at the QCP, which provides strong evidence of a critical dipole liquid with a Bose surface, UV-IR mixing, and a dispersion relation  $\omega = k_x k_y$ .

DOI: [10.1103/PhysRevB.106.235130](https://doi.org/10.1103/PhysRevB.106.235130)

### I. INTRODUCTION

After a decade of intense effort focused on topological materials, a new class of symmetry-protected topological insulators, dubbed higher-order topological insulators (HOTIs), has been discovered [1–4]. HOTIs admit gapped surfaces separated by gapless corners/hinges where the surfaces intersect and exemplify a rich bulk-boundary correspondence. Aside from HOTIs generated by topological band structures, recent research suggests that strongly interacting bosonic systems can potentially host a HOTI having robust bosonic corner zero modes [5,6]. Now the characterization of interacting HOTIs has been widely explored in terms of mathematical invariants, topological response, and field theory approaches [7,8]. However, the existence and character of a quantum phase transition between an interacting HOTI phase and a trivial Mott insulator phase is still nebulous. In particular, it is noteworthy to explore whether the critical region inherits the topological properties of the HOTI, and how such a phase transition is influenced by the topological structure, and the entanglement pattern, of the adjacent HOTI phase.

In this work, we address these questions and propose a different type of quantum critical point that connects a two-dimensional (2D) HOTI phase [8,9] and a trivial Mott insulator phase. The traditional guiding principle behind the modern theory of critical phenomena, known as the Ginzburg-Landau-Wilson (GLW) paradigm, is the identification of an “order parameter fluctuation” that encapsulates the differ-

ences in symmetry between the two phases proximate to the critical point. However, the quantum critical point (QCP) that we present in this paper eludes this paradigm as both the HOTI phase and the trivial Mott phase have the same symmetries and are distinguished only through their different topological character.

Remarkably, we find that the phase transition that we propose inherits topological features from the HOTI phase. The QCP can be understood as the bulk percolation [10] of domain walls that act as phase boundaries between regions containing a HOTI or trivial Mott insulator. The corners and rough patches of the 1D domain walls can be treated as the corners of the HOTI phase, and are thus each decorated with a robust spinon zero mode. At the QCP, the proliferation of domain walls triggers the fluctuations of the corner zero modes and precipitates fracton dynamics of the spinons that are constrained by subsystem U(1) symmetry. Hence, we find that this critical point contains quasiparticles with fracton behavior and subdimensional kinetics where the spinon dipoles only move transverse to their dipole moment [11–28]. This type of quantum criticality leads us to propose that the phase transition is characterized by a critical dipole liquid [25,29–32]. This critical theory has several key features including: (i) a Bose surface [33] having zero energy states that form closed nodal lines along the  $k_x$  and  $k_y$  axes, and (ii) a breakdown in the area law of the entanglement entropy, which is replaced by a scaling with a logarithmic enhancement  $L \ln(L)$  at the critical point instead. (iii) The phase transition theory is subject to UV-IR mixing as the critical point

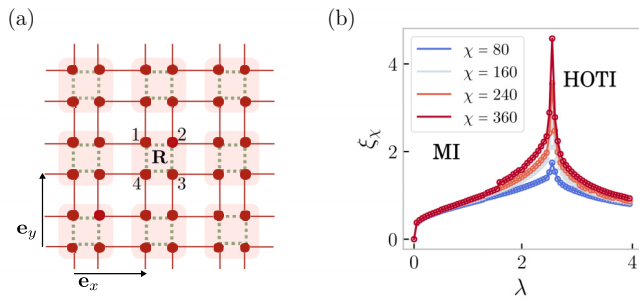


FIG. 1. Lattice model and quantum critical point (QCP). (a) The lattice model. Each unit cell consists of four spin  $S = 1/2$  (red dots). The ring-exchange terms (red squares) couple four neighboring unit cells, while sites in the unit cell are isotropically coupled via an  $XY$  interaction (green dotted lines). (b) The correlation length  $\xi_\chi$  as a function of the tuning parameter  $\lambda$  and the bond dimension  $\chi$  for an infinite cylinder along  $x$ ,  $L_x = \infty$ , and periodic boundary conditions along  $y$  with a circumference  $L_y = 6$ . A second-order quantum phase transition between a Mott insulator (MI) and higher-order topological insulator (HOTI) occurs at  $\lambda_c \approx 2.54$ .

is controlled by shortwave length modes with strong local fluctuations.

## II. LATTICE MODEL AND PHASE DIAGRAM

To frame our discussion, we consider the following model on a 2D square lattice with four spin-1/2 degrees of freedom per unit cell:

$$\begin{aligned}
 H &= H_{XY} - \lambda H_{\text{ring exchange}} \\
 &= \sum_{\mathbf{R}} (S_{\mathbf{R},1}^+ S_{\mathbf{R},2}^- + S_{\mathbf{R},2}^+ S_{\mathbf{R},3}^- + S_{\mathbf{R},3}^+ S_{\mathbf{R},4}^- + S_{\mathbf{R},4}^+ S_{\mathbf{R},1}^-) \\
 &\quad - \lambda \sum_{\mathbf{R}} (S_{\mathbf{R},2}^+ S_{\mathbf{R}+\mathbf{e}_x,1}^- S_{\mathbf{R}+\mathbf{e}_x+\mathbf{e}_y,4}^+ S_{\mathbf{R}+\mathbf{e}_y,3}^-) + \text{H.c.} \quad (1)
 \end{aligned}$$

Hamiltonian (1) contains an intercell ring-exchange interaction between the four spins located at the four corners of each red plaquette, and an  $XY$  spin interaction within the unit cell, as shown in Fig. 1(a). In passing, we mention that models having ring-exchange terms of this type can be realized in cold-atom settings, which hence is a natural arena for the experimental investigation of our subsequent predictions [34,35]. The magnon creation/annihilation operators  $S^\pm = \sigma^x \pm i\sigma^y$  can be mapped to a hardcore boson description using  $b^\dagger(b) = S^+(S^-)$ ,  $S^z = n_b - 1/2$ , where  $n_b = b^\dagger b$ ; we use both languages interchangeably where convenient. Equation (1) exhibits time-reversal  $\mathcal{T} = \prod_{\mathbf{R}} \prod_{m=1}^4 i\sigma_{\mathbf{R},m}^y \mathcal{K}$  symmetry and a subsystem  $U(1)$  symmetry that conserves the sum of  $S^z$  inside the unit cell  $\mathbf{R}$ , i.e.,  $S^z(\mathbf{R}) = \sum_{m=1}^4 S_{\mathbf{R},m}^z$ , for every row ( $\mathbf{R}$ ) and column ( $\mathbf{C}$ ),

$$U_{R(C)}^{\text{sub}}(1) : \prod_{\mathbf{R} \in R(C)} e^{i\theta S^z(\mathbf{R})}. \quad (2)$$

The subsystem  $U(1)$  symmetry restricts the mobility of the magnon, and hence the leading-order dynamics are attributed to pairs of dipoles, each composed of a particle-hole pair on a lattice link, that hop along the direction transverse to their dipole moment.

Before turning to the detailed study of the phase diagram for the model given by Eq. (1), let us discuss two exactly solvable limits. As  $\lambda$  is tuned, the system effectively has competing orders dominated by either the intracell  $XY$  interaction or the intercell plaquette ring-exchange interaction. In the limit  $\lambda \sim 0$ , the intracell term plays the key role and generates an entangled cluster within each unit cell. The resulting ground state, which is simply a tensor product of the ground state of each unit cell, is a featureless Mott insulator with a magnon gap for both the bulk and boundary. In the opposite limit  $\lambda \sim \infty$ , it was shown in Ref. [8] that the plaquette term projects the four interacting spins into a unique maximally entangled state  $|\downarrow_2 \uparrow_1 \downarrow_4 \uparrow_3\rangle + |\uparrow_2 \downarrow_1 \uparrow_4 \downarrow_3\rangle$  where we omitted unit cell labels. The corresponding ground state for the entire system is thus a product of entangled plaquettes and has a finite magnon gap in the bulk. In the presence of a smooth boundary, each edge unit cell naively has two free spin-1/2 modes, but these can be coupled and gapped to form a singlet state via the on-site  $XY$  coupling in Eq. (1) (even for infinitesimal  $\lambda$ ). For rough edges and/or corners, there is an additional spin-1/2 zero mode per corner whose twofold degeneracy is protected by both  $\mathcal{T}$  and subsystem  $U(1)$  symmetry, so the resultant state renders a higher-order topological insulator. This subsystem symmetric HOTI phase was studied in Ref. [8] and was shown to exhibit a quantized quadrupole moment density of  $Q_{xy} = 1/2$ .

We obtained the phase diagram [Fig. 1(b)] using the density matrix renormalization group (DMRG) method [36–38] on an infinitely long cylinder. We find that the aforementioned limits extend into two gapped phases (a trivial Mott insulator and a HOTI, respectively). Importantly, our numerics indicate that the two gapped phases are connected by a second-order phase transition at  $\lambda_c \approx 2.54$ . It is noteworthy to emphasize that the HOTI phase and the trivial Mott phase display the same symmetries, but harbor distinct topological features, and thus cannot be differentiated via any local observable. This further implies that the QCP between the phases is beyond the GLW paradigm.

## III. DESCRIPTION OF THE QUANTUM CRITICAL POINT

We now provide both an analytic argument and numerical evidence to demonstrate that the quantum critical point separating the HOTI phase and the trivial Mott phase displays gapless fracton quasiparticles akin to a critical dipole liquid. When the interaction strength  $\lambda$  is comparable to the intracell tunneling strength, the plaquette entangled patterns and on-site entangled patterns compete and coexist in the bulk. The coexistence and spatial phase separation can be viewed from a percolation picture, illustrated in Fig. 2. In the quantum critical region adjacent to the trivial Mott phase, the plaquette ring-exchange term triggers some regions containing plaquette entangled states that exhibit the HOTI ground-state pattern. Domain walls that form between the two phases can be viewed as the boundary between the HOTI and trivial phases, and hence they harbor a spinon zero mode at each corner (and each ‘‘rough’’ patch on the edges). In the quantum critical region, strong fluctuations between different phase separation patterns are induced, and the domain walls tend to proliferate. These spatial fluctuations concurrently trigger the dynamics

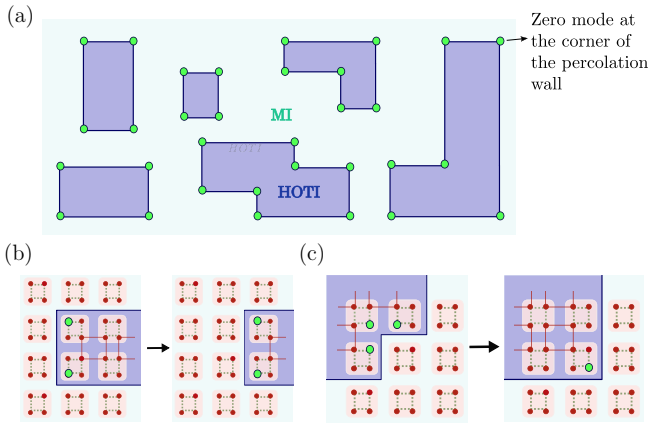


FIG. 2. (a) At the critical point, the HOTI (blue shaded area) and trivial Mott insulator (green shaded region) coexist and their phase boundary (domain wall) contains spinon zero modes (green dot) at the corners. (b),(c) The spatial fluctuation of phase boundaries (domain walls) induces motion for the spinon pairs at neighboring corners.

of the spinon zero modes on the corners of the domain walls, similar to the percolation of domain wall defects in 1D [10].

More precisely, the spinon dynamics originates from the resonance between distinct percolation patterns. In Figs. 2(b) and 2(c), we display two typical phase boundary deformations. By shrinking a stripe domain along the  $x$  direction, the two spinon zero modes forming an effective  $y$ -oriented dipole can hop along the  $x$  direction, and vice versa. This motion can be described by a ring-exchange term for the spinons,

$$\sum_{i=1}^2 z_i^\dagger(\mathbf{R}) z_i(\mathbf{R} + \mathbf{e}_x) z_i^\dagger(\mathbf{R} + \mathbf{e}_x + \mathbf{e}_y) z_i(\mathbf{R} + \mathbf{e}_y), \quad (3)$$

where  $(z_1^\dagger, z_2^\dagger)$  is the  $CP^1$  representation of the spinon with  $S_i^z = \frac{1}{2} z_i^\dagger \sigma_{ij}^z z_j$ . Another typical domain wall deformation occurs when a corner is shrunk by removing a corner plaquette from the stripe. This effectively removes the free spinon from the corner, but it also creates three other spinons at the newly created corners. This process is also represented by the ring-exchange term in Eq. (3). Hence, the spatial fluctuations of the percolating domain walls generate a ring-exchange type term for spinons that effectively corresponds to the motion of dipoles transverse to their dipole moment. An important characteristic of this transition is that the percolation at the QCP does not trigger the hopping of a single spinon, stemming from the fact that the spinon modes on the phase boundaries are localized at the corners.

Based on these key observations, we propose that the low-energy effective description of the QCP is a critical dipole liquid theory,

$$\mathcal{L} = \sum_{\gamma=1,2} (\partial_t \theta_\gamma + a_0)^2 - K (\partial_x \partial_y \theta_\gamma + a_{xy})^2, \\ a_{xy} \rightarrow a_{xy} + \partial_x \partial_y \alpha, \quad a_0 \rightarrow a_t + \partial_t \alpha, \quad z_i^\dagger = n_i e^{i\theta_i}. \quad (4)$$

Here we used a number-phase representation for the  $CP^1$  spinons, and  $a_0, a_{xy}$  are components of the emergent gauge field that couple to the gauge charge of the spinon; their gauge transformations are also listed above. We note that we are ignoring the compactification of the boson fields  $\theta_i$ , and have expanded to quadratic order in them [25]. The legitimacy of this approximation, which is tied to the irrelevance of instanton tunneling events, is discussed in detail in the Supplemental Material [39]. To further analyze this theory, we can decompose the two  $CP^1$  phase fields as  $\theta_\pm = \theta_1 \pm \theta_2$  to find

$$\mathcal{L} = \frac{1}{2} \sum_{\gamma=\pm} (\partial_t \theta_\gamma)^2 - \frac{K}{2} (\partial_x \partial_y \theta_+ + a_{xy})^2 - \frac{K}{2} (\partial_x \partial_y \theta_-)^2. \quad (5)$$

We find that the field  $\theta_+$  is the only bosonic spinon mode that couples to the emergent gauge field  $a_{xy}$ . Hence this mode is gapped out due to a Higgs-like mechanism for the gauge field or, equivalently, by the on-site  $XY$  interaction (see the Supplemental Material [39] for details). The field  $\theta_-$  denotes the gapless magnon mode,  $S^\pm = e^{i\pm\theta_-}$ , that carries the  $S_z$  quantum number. This field contributes to the low-energy dynamical phenomena at quantum criticality, and henceforth we only focus on the  $\theta_-$  branch.

Due to subsystem  $S_z$  conservation, the action in Eq. (5) is invariant under a special  $U(1)$  transformation,  $\theta_- \rightarrow \theta_- + f(x) + g(y)$ . Consequently, the single magnon hopping term  $(\partial_t \theta_-)^2$  is forbidden as it breaks this subsystem  $U(1)$  symmetry explicitly. Instead, the leading-order dynamics originates from dipole moments oriented along the  $i$ th direction, i.e.,  $(\partial_t \theta_-)$ , that are constrained to move along the transverse  $j$ th direction. This is captured in our theory by a special, higher-order kinetic term  $(\partial_j \partial_t \theta_-)^2$  yielding a dispersion  $\omega \sim k_x k_y$ . This is remarkable because we find that the QCP exhibits characteristic fractonic features arising from a percolation process where the corner-localized low-energy modes cannot fluctuate independently without creating additional corners. Finally, we note that this theory can also be used to describe the gapped phases proximate to the QCP (see Supplemental Material [39] for details).

An alternative way to illustrate the fracton dynamics at the critical point is to explore the magnon dynamics directly from the microscopic Hamiltonian in Eq. (1). When the interaction strength  $\lambda$  grows, the intercell coupling term triggers the magnons to fluctuate between unit cells. However, as the intercell coupling contains only a ring-exchange term, it does not support single charge hopping between cells and hence the leading-order dynamics is governed by a pair of magnon dipoles hopping between cells [30,31,40,41]. To corroborate this, we find that the two-point correlator  $\langle S^+(\mathbf{R}) S^-(\mathbf{R}) \rangle$  is short ranged at the QCP. In contrast, since we expect that the critical region manifests a critical dipole liquid, we find that the four-point correlation functions between two spin-dipoles living on the same transverse stripe are [25],

$$\langle S^+(\mathbf{R}) S^-(\mathbf{R} + \mathbf{e}_y) S^-(\mathbf{R} + x) S^+(\mathbf{R} + x + \mathbf{e}_y) \rangle = \frac{1}{(x)^{1/(K\pi^2)}}, \quad (6)$$

and analogously for a stripe along  $y$ . These correlation functions exhibit algebraic decay and quasi-long-range order if and only if the two dipoles are living on the same stripe. This

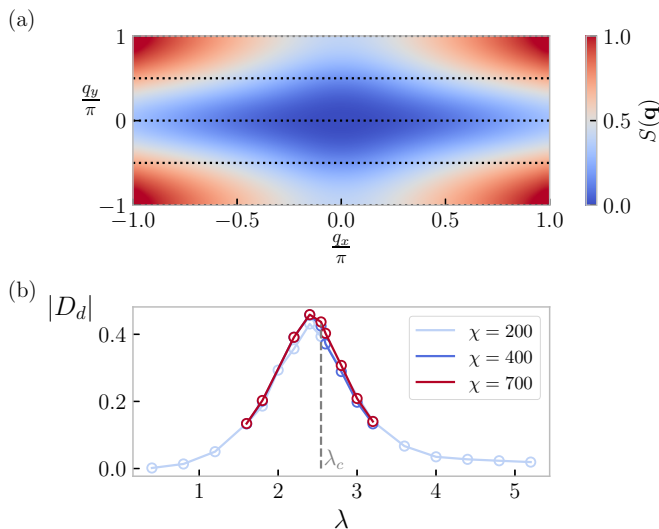


FIG. 3. Static structure factor and dipole stiffness. (a) The static structure factor  $S(\mathbf{q})$  calculated for a stripe with  $L_x = 100$  and  $L_y = 8$  sites along the  $x$  and  $y$  direction, respectively. Hence, the data are obtained for momenta  $q_y = 0, \pm\pi, \pm\pi/2$  (black, dotted lines). (b) The absolute value of the dipole stiffness  $|D_d|$ , calculated for an infinite cylinder with  $L_y = 6$ . The dipole stiffness is obtained by taking the second, symmetric derivative with step size  $\delta\Phi = 0.05$ .

again supports the fact that we should interpret the critical point as a dipole liquid having constrained subsystem dynamics.

As a further confirmation of the dipole liquid critical point, we characterize the dipole liquid by its transport properties since our model has dipole conservation. In the language of Ref. [42], we expect the critical dipole liquid to act as a “dipole metal” and exhibit a nonvanishing dipole conductivity in the presence of a uniform rank-2 electric field, e.g.,  $E_{xy}$ . In analogy to Kohn’s criterion on defining conductors and insulators [43], Ref. [42] proposed a criterion to establish the existence of a dipole metal based on the dipole stiffness  $D_d$  (details of its definition and calculation can be found in the Supplemental Material [39]), suggesting that if  $D_d$  is nonvanishing in the thermodynamic limit, then the system is a dipole metal. Our results for  $D_d$  are shown in Fig. 3(b) and we find that they clearly support our theory since the system shows a nonvanishing  $D_d$  only in the neighborhood of the critical point.

#### IV. FEATURES OF THE QUANTUM CRITICAL POINT

Now let us consider several remarkable properties of this critical point. The critical theory in Eq. (5) produces a quadratic dispersion  $\omega \sim k_x k_y$ , which implies a Bose surface with characteristic lines of zero-energy modes on both the  $k_x$  and  $k_y$  axes. For each fixed momentum slice  $k_i \neq 0$ , the low-energy dispersion is akin to the 1D relativistic boson along the transverse direction. Such “quasi-1D” motion is a consequence of the subdimensional nature of the critical dipole liquid, i.e., the fact that an  $x(y)$ -oriented dipole is only mobile along the transverse  $y(x)$ -oriented stripes. To confirm the existence of the Bose surface, we numerically evaluate the

structure factor,

$$S(\mathbf{q}) = \frac{1}{N} \left[ \prod_{m=1}^2 \sum_{\mathbf{R}_m, \mathbf{b}_m} e^{i\mathbf{q} \cdot [(-1)^m \mathbf{\Lambda}_m]} \right] \langle S_{\mathbf{\Lambda}_1}^z, S_{\mathbf{\Lambda}_2}^z \rangle, \quad (7)$$

where  $N = L_y L_x / 4$  is the total number of unit cells, and  $\mathbf{\Lambda}_m = \mathbf{R}_m + \mathbf{b}_m$  specifies one of the four spins  $S_{\mathbf{R}_m, m}^z$  inside the unit cell  $\mathbf{R}_m$  with basis vectors  $\mathbf{b}_m \in \frac{1}{2} \{ \mathbf{0}, \mathbf{e}_x, \mathbf{e}_y, \mathbf{e}_x + \mathbf{e}_y \}$ . In Fig. 3(a), we show that the numerically obtained structure factor exhibits clear zero-energy lines along the  $k_x, k_y$  axes. Furthermore, each  $k_i \neq 0$  exhibits dispersion like a 1D relativistic boson along the transverse direction. We note that since there are nodal lines at  $k_x, k_y = 0$ , there is a subextensive number of quasi-1D modes, and the specific heat at low temperature will scale as  $C_v \sim T \ln(1/T)$ , which is similar to marginal Fermi liquid theory in 2D [25,29,30]. Remarkably, as a subextensive number of zero-energy modes survive at high momentum, the resultant theory is controlled and crucially depends on short-wavelength modes that generate strong local fluctuations. Such a critical theory is triggered by short-wavelength physics and is subject to UV-IR mixing [41] (see Supplemental Material [39] for more details).

Indeed, another noteworthy feature for the critical dipole liquid is an unusually large entanglement entropy scaling that exceeds the area law. In conventional 2D quantum critical points, despite the divergent correlation length, the entanglement entropy of the ground state carried by a subregion of the many-body system is still local in the sense that it scales with  $L$ , the perimeter of the subsystem boundary. However, in the critical theory we present here, the entanglement entropy should scale with the subregion size as  $L \ln(L)$  [44,45]. Such a violation of the area law can be substantiated by dividing the Bose surface into small patches over which the surface looks approximately flat. Each patch can be regarded as a 1D relativistic boson whose entanglement entropy scales as  $\ln(L)$ . Summing over the contributions from all patches, the total entanglement entropy should scale as  $L \ln(L)$ . This represents an observation of a 2D quantum critical point whose entanglement pushes beyond the area law. This implies that the critical dipole liquid has long-range mutual information shared by two regions that are far apart.

In conclusion, we provided a framework to describe a type of 2D quantum criticality with logarithmic entanglement scaling and emergent fracton dynamics in the absence of Lorentz invariance. Our description of the HOTI percolation transition also suggests insights for various topological phase transitions and critical points beyond the GLW paradigm, and is certain to have rich theoretical and experimental implications perhaps in near-term cold-atom experiments.

#### ACKNOWLEDGMENTS

This work was initiated at KITP. Y.Y., T.L.H., and F.P. are supported in part by the National Science Foundation under Grant No. NSF PHY-1748958 (KITP) as part of the Topological Quantum Matter program. F.P. acknowledges the support of the DFG Research Unit FOR 1807 through Grants No. PO 1370/2-1 and No. TRR80, and the

Deutsche Forschungsgemeinschaft (DFG, German Research Foundation) under Germany's Excellence Strategy Grant No. EXC-2111-390814868. T.L.H. thanks the U.S. National Sci-

ence Foundation (NSF) MRSEC program for support under NSF Award No. DMR-1720633 (SuperSEED) and Award No. DMR 1351895-CAR.

- 
- [1] W. A. Benalcazar, B. A. Bernevig, and T. L. Hughes, *Science* **357**, 61 (2017).
- [2] F. Schindler, A. M. Cook, M. G. Vergniory, Z. Wang, S. S. Parkin, B. A. Bernevig, and T. Neupert, *Sci. Adv.* **4**, eaat0346 (2018).
- [3] J. Langbehn, Y. Peng, L. Trifunovic, F. von Oppen, and P. W. Brouwer, *Phys. Rev. Lett.* **119**, 246401 (2017).
- [4] Z. Song, Z. Fang, and C. Fang, *Phys. Rev. Lett.* **119**, 246402 (2017).
- [5] Y. You, T. Devakul, F. J. Burnell, and T. Neupert, *Phys. Rev. B* **98**, 235102 (2018).
- [6] O. Dubinkin and T. L. Hughes, *Phys. Rev. B* **99**, 235132 (2019).
- [7] A. Rasmussen and Y.-M. Lu, *Phys. Rev. B* **101**, 085137 (2020).
- [8] Y. You, F. Burnell, and T. L. Hughes, *Phys. Rev. B* **103**, 245128 (2021).
- [9] J. Bibo, I. Lovas, Y. You, F. Grusdt, and F. Pollmann, *Phys. Rev. B* **102**, 041126 (2020).
- [10] X. Chen, F. Wang, Y.-M. Lu, and D.-H. Lee, *Nucl. Phys. B* **873**, 248 (2013).
- [11] C. Chamon, *Phys. Rev. Lett.* **94**, 040402 (2005).
- [12] J. Haah, *Phys. Rev. A* **83**, 042330 (2011).
- [13] B. Yoshida, *Phys. Rev. B* **88**, 125122 (2013).
- [14] S. Vijay, J. Haah, and L. Fu, *Phys. Rev. B* **94**, 235157 (2016).
- [15] M. Pretko, X. Chen, and Y. You, [arXiv:2001.01722](https://arxiv.org/abs/2001.01722).
- [16] H. Ma, E. Lake, X. Chen, and M. Hermele, *Phys. Rev. B* **95**, 245126 (2017).
- [17] M. Pretko and L. Radzihovsky, *Phys. Rev. Lett.* **120**, 195301 (2018).
- [18] M. Pretko, *Phys. Rev. B* **96**, 035119 (2017).
- [19] M. Pretko, *Phys. Rev. B* **95**, 115139 (2017).
- [20] D. Bulmash and M. Barkeshli, [arXiv:1806.01855](https://arxiv.org/abs/1806.01855).
- [21] A. Gromov, A. Lucas, and R. M. Nandkishore, *Phys. Rev. Res.* **2**, 033124 (2020).
- [22] A. Gromov, *Phys. Rev. X* **9**, 031035 (2019).
- [23] H. Ma and M. Pretko, *Phys. Rev. B* **98**, 125105 (2018).
- [24] W. Shirley, K. Slagle, and X. Chen, *Ann. Phys.* **410**, 167922 (2019).
- [25] Y. You, Z. Bi, and M. Pretko, *Phys. Rev. Res.* **2**, 013162 (2020).
- [26] A. Prem, M. Pretko, and R. Nandkishore, *Phys. Rev. B* **97**, 085116 (2018).
- [27] R. M. Nandkishore and M. Hermele, *Annu. Rev. Condens. Matter Phys.* **10**, 295 (2019).
- [28] J. Feldmeier, P. Sala, G. De Tomasi, F. Pollmann, and M. Knap, *Phys. Rev. Lett.* **125**, 245303 (2020).
- [29] C. Xu and M. P. A. Fisher, *Phys. Rev. B* **75**, 104428 (2007).
- [30] A. Paramekanti, L. Balents, and M. P. A. Fisher, *Phys. Rev. B* **66**, 054526 (2002).
- [31] T. Tay and O. I. Motrunich, *Phys. Rev. Lett.* **105**, 187202 (2010).
- [32] R. V. Mishmash, M. S. Block, R. K. Kaul, D. N. Sheng, O. I. Motrunich, and M. P. A. Fisher, *Phys. Rev. B* **84**, 245127 (2011).
- [33] S. Sachdev, *Nature (London)* **418**, 739 (2002).
- [34] B. Paredes and I. Bloch, *Phys. Rev. A* **77**, 023603 (2008).
- [35] H.-N. Dai, B. Yang, A. Reingruber, H. Sun, X.-F. Xu, Y.-A. Chen, Z.-S. Yuan, and J.-W. Pan, *Nat. Phys.* **13**, 1195 (2017).
- [36] S. R. White, *Phys. Rev. Lett.* **69**, 2863 (1992).
- [37] I. P. McCulloch, [arXiv:0804.2509](https://arxiv.org/abs/0804.2509).
- [38] J. Hauschild and F. Pollmann, *SciPost Phys. Lect. Notes* **5** (2018).
- [39] See Supplemental Material at <http://link.aps.org/supplemental/10.1103/PhysRevB.106.235130> for additional details of the calculations from the main article.
- [40] C. D. Batista and Z. Nussinov, *Phys. Rev. B: Condens. Matter* **72**, 045137 (2005).
- [41] N. Seiberg and S.-H. Shao, *SciPost Phys.* **9**, 046 (2020).
- [42] O. Dubinkin, J. May-Mann, and T. L. Hughes, *Phys. Rev. B* **103**, 125129 (2021).
- [43] W. Kohn, *Phys. Rev.* **133**, A171 (1964).
- [44] H.-H. Lai, K. Yang, and N. E. Bonesteel, *Phys. Rev. Lett.* **111**, 210402 (2013).
- [45] B. Swingle, *Phys. Rev. Lett.* **105**, 050502 (2010).